Supporting Information – Solvation at metal/water interfaces: An ab initio molecular dynamics benchmark of common computational approaches

Hendrik H. Heenen,[†] Josef A. Gauthier,[‡] Henrik H. Kristofferson,[†] Thomas Ludwig,[‡] and Karen Chan[*,†]

†*Department of Physics, Technical University of Denmark, DK-2800, Kgs. Lyngby, Denmark*

‡*SUNCAT Center for Interface Science and Catalysis, Department of Chemical Engineering, Stanford University, Stanford, California 94305, United States*

¶*SUNCAT Center for Interface Science and Catalysis, SLAC National Accelerator Laboratory, 2575 Sand Hill Road, Menlo Park, California 94025, United States*

E-mail: kchan@fysik.dtu.dk

I Convergence of *ab initio* Molecular Dynamics

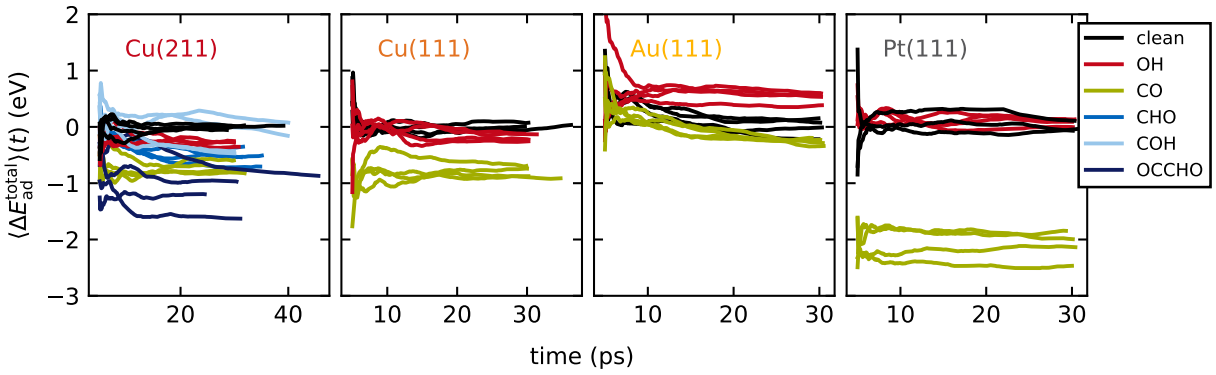

Figure S1: Total average adsorption energy (eq. 1 main text) against simulation time $\langle \Delta E_{\mathrm{ad}}^{\mathrm{total}} \rangle (t)$ (cumulative average) after the equilibration period of 5 ps for all individual trajectories. The shown energies are of the uncorrected trajectories including chemical reactions (see main text). The gas phase references are kept constant for all time steps.

Table S1: Total average adsorption energy (eq. 1 main text) $\langle \Delta E_{\mathrm{ad}}^{\mathrm{total}} \rangle (t)$ and drift in total energy $\frac{dE^{\mathrm{total}}}{dt}$ (meV/ps) for the four individual trajectories of each system after 5 ps equilibration and at least 25 ps sampling time.

system	$\langle \Delta E_{\mathrm{ad}}^{\mathrm{total}} \rangle$ (eV)				$\frac{dE^{\mathrm{total}}}{dt}$ (meV/ps)			
	#1	#2	#3	#4	#1	#2	#3	#4
Cu211	-0.06	0.02	0.01	0.03	-7	6	9	-4
OH/Cu211	-10.87	-10.94	-10.84	-10.86	-5	-8	-7	2
CO/Cu211	-15.13	-15.03	-15.16	-14.93	1	-8	-1	13
CHO/Cu(211)	-18.31	-18.16	-18.51	-18.34	1	7	-12	-29
COH/Cu211	-17.97	-17.73	-18.25	-18.28	-31	-14	-24	-20
OCCHO/Cu211	-33.05	-33.38	-33.15	-33.81	-23	6	-8	-10
Cu111	0.07	-0.12	0.01	0.03	-1	-12	17	11
OH/Cu(111)	-10.81	-10.72	-10.85	-10.71	-7	-14	-3	-12
CO/Cu111	-15.21	-15.08	-15.03	-15.25	1	16	-20	-7
Pt111	-0.04	-0.07	0.11	0.03	13	-22	-29	-11
OH/Pt(111)	-10.46	-10.45	-10.50	-10.59	-10	3	-7	2
CO/Pt111	-16.18	-16.47	-16.33	-16.80	11	5	-21	1
Au(111)	0.15	0.08	-0.22	-0.01	-2	-21	-28	-2
OH/Au(111)	-9.99	-10.20	-10.06	-10.00	-2	0	-12	-19
CO/Au111	-14.62	-14.68	-14.57	-14.53	-21	-45	-22	-4

II Metal-water radial distribution functions

We monitor the metal-water interface via a radial distribution function (RDF) between the top-layer metal atoms (Me) and the hydrogen (H) and oxygen atoms (O) of the water molecules. This delivers a complementary picture to the density profiles presented in Sec. III A in the main text.

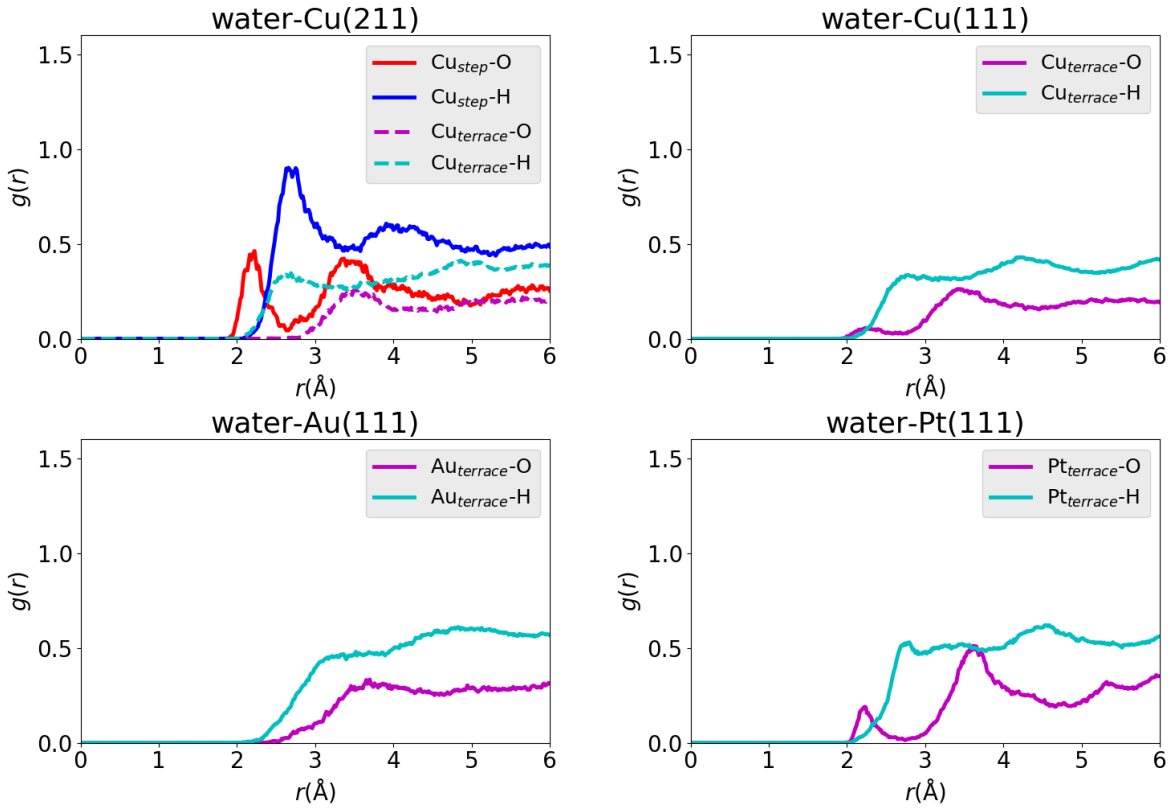

Figure S2: Radial distribution function $g(r)$ of the Me-O_{H_2O} distance with Me = Cu(211) (top left), Cu(111) (top right), Au(111) (bottom left), and Pt(111) (bottom right).

As shown in Fig. S2, the Me-O RDFs of the Cu(211), Cu(111), and Pt(111) surfaces show a water-bilayer structure visible through a double peak at r=2-4 Å. While this is also reflected in the density profiles of Cu(111) and Pt(111) (see main text), it is not obvious in the density profile of Cu(211). For the latter, it can be seen that the bilayer structure forms primarily around the step edge. We use the RDFs to determine a criterion for water adsorption. In that, 2.55 Å is chosen, which is the distance including the first bilayer peak for the Cu and Pt surface and the onset of the water boundary on Au(111).

III Binding and solvation energies

The adsorption and solvation energies obtained through geometry optimizations in presence (and absence) of implicit solvent for all adsorbate/surface combinations are depicted in Tab. S2, S3, and S4. Included are all sites which were sampled during the respective AIMD simulations. The labeling of the symmetrically inequivalent sites of same coordination symmetry follows alphabetical order. That means, that among all top, bridge, threefold hollow (hollow3) or fourfold hollow (hollow4) sites a tag "-a", "-b", ... is introduced (c.f. Fig. S3).

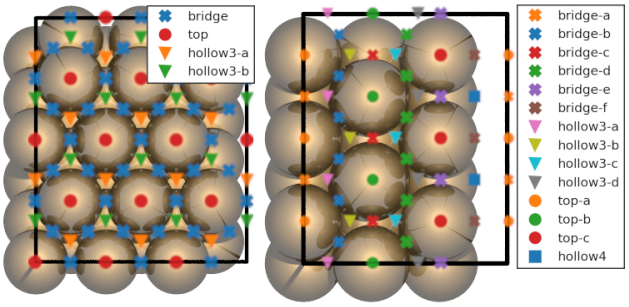

Figure S3: Surface sites for the 3×4-(111) (left) and 3×1-(211) (right) slab models used for the site-partitioning of the AIMD trajectories. Symmetrically equivalent sites are shown in the same color.

It can be seen in Tab. S2, S3, and S4 that in most cases the relative share of occupation during an AIMD trajectory r_{site} matches the relative stability of the respective site obtained from the geometry optimization.

In order to generalize the findings for the density based (GLSSA13)[1] implicit solvent model as implemented in VASPsol,[2] we evaluate all adsorption and solvation energies based on Quantum ESPRESSO / Environ.[3,4] For this, we employ geometry optimizations in presence and absence of the self-consistent continuum solvation (SCCS) implicit solvent model on the same adjusted slab models. The computational details are kept equivalent where possible, with the same RPBE-D3 functional[5–7] and using the same Monkhorst-Pack k-point grids. Otherwise, plane-wave and density cutoffs of 500 and 5000 eV and a Fermi-smearing width of 0.1 eV were used. The electronic structure was converged until a total energy dif-

Table S2: Adsorption and solvation energies (ΔE_{ad} and ΔE_{sol}) computed via geometry optimizations at all adsorption sites probed during the AIMD simulations. Additional to the VASPsol results (see main text) the optimized energies in Quantum ESPRESSO / Environ (QE-SCCS) are depicted. The overall site-occupation ratio r_{site} and the residence time τ during the AIMD simulations for each site are shown as well. See Fig. S3 for an explanation of the site labels.

	$\Delta E_{\mathrm{ad}}^{\mathrm{VASPsol}}$	$\Delta E_{\mathrm{sol}}^{\mathrm{VASPsol}}$	$\Delta E_{\mathrm{ad}}^{\mathrm{QE\text{-}SCCS}}$	$\Delta E_{\mathrm{sol}}^{\mathrm{QE\text{-}SCCS}}$	r_{site}	τ (ps)
	OH / Cu(211)					
hollow3-d	-0.53	-0.12	-0.27	-0.07	0.01	192.50
bridge-e	-0.52	-0.10	-0.51	-0.10	0.97	4434.14
top-c	-0.52	-0.09	-0.50	-0.11	0.01	336.00
hollow4	-0.52	-0.09	-0.50	-0.10	0.01	177.00
	CO / Cu(211)					
top-c	-0.97	0.00	-0.93	0.00	0.12	596.88
bridge-f	-0.95	0.00	-0.89	0.00	0.01	228.50
hollow3-c	-0.94	-0.01	-0.88	0.00	0.03	481.04
bridge-d	-0.94	-0.01	-0.88	0.00	0.10	238.02
hollow3-d	-0.94	0.00	-0.87	0.00	0.29	393.13
bridge-e	-0.94	0.00	-0.93	0.00	0.43	761.52
bridge-c	-0.93	-0.01	-0.88	0.00	0.01	0.00
	COH / Cu(211)					
bridge-a	0.00	-0.02	0.12	-0.09	0.13	220.00
hollow4	0.00	-0.13	0.14	-0.18	0.87	515.78

ference of 10^{-5} eV. For the employed slab models, the lattice constants are adjusted based on the computational details and converged to 3.694 Å for Cu, 4.229 Å for Au, and 4.018 Å for Pt.

The adsorption energies obtained from the two employed DFT codes are in most cases very similar and only differ in some cases with a maximum deviation of ≤ 0.2 eV. We attribute these deviations to the difference in the PAW-formalism in VASP and the employed ultra-soft pseudopotentials. In contrast to this, the contribution of the implicit solvent model and thus the solvation energies are near-identical. This indicates, that the here presented shortcomings for continuum solvation methods are of general nature. It should be noted, that we omitted more rigorous solvation schemes like RISM or CANDLE (see main text). These may account for some of the directional contributions and thus improve the continuum

Table S3: Adsorption and solvation energies (ΔE_{ad} and ΔE_{sol}) computed via geometry optimizations at all adsorption sites probed during the AIMD simulations. Additional to the VASPsol results (see main text) the optimized energies in Quantum ESPRESSO / Environ (QE-SCCS) are depicted. The overall site-occupation ratio r_{site} and the residence time τ during the AIMD simulations for each site are shown as well. See Fig. S3 for an explanation of the site labels.

	$\Delta E_{\mathrm{ad}}^{\mathrm{VASPsol}}$	$\Delta E_{\mathrm{sol}}^{\mathrm{VASPsol}}$	$\Delta E_{\mathrm{ad}}^{\mathrm{QE\text{-}SCCS}}$	$\Delta E_{\mathrm{sol}}^{\mathrm{QE\text{-}SCCS}}$	r_{site}	τ (ps)
	CHO / Cu(211)					
hollow4	-0.66	-0.09	-0.53	-0.09	0.02	316.58
bridge-b	-0.62	-0.11	-0.53	-0.09	0.10	266.25
bridge-d	-0.61	-0.08	-0.52	-0.08	0.00	218.00
top-c	-0.61	-0.12	-0.52	-0.10	0.16	474.83
bridge-f	-0.56	-0.10	-0.49	-0.09	0.03	380.83
top-b	-0.51	-0.08	-0.35	-0.08	0.34	481.11
bridge-e	-0.51	-0.08	-0.30	-0.06	0.28	668.26
bridge-c	-0.51	-0.08	-0.30	-0.06	0.03	158.50
hollow3-b	-0.48	-0.09	-0.39	-0.09	0.03	342.67
hollow3-d	-0.41	-0.03	-0.34	-0.04	0.00	0.00
hollow3-c	-0.37	-0.04	-0.29	-0.04	0.00	0.00
	OCCHO / Cu(211)					
bridge-d	-1.31	-0.16	-1.17	-0.12	0.06	439.23
hollow3-c	-1.30	-0.17	-1.13	-0.10	0.02	866.00
top-c	-1.29	-0.15	-1.17	-0.14	0.23	643.89
bridge-e	-1.27	-0.15	-1.20	-0.13	0.65	3488.03
bridge-f	-1.22	-0.19	-1.00	-0.01	0.01	324.33
hollow3-d	-1.18	-0.05	-1.05	-0.10	0.02	253.88
bridge-b	-1.16	-0.17	-1.02	-0.13	0.03	0.00

solvation energies.

Table S4: Adsorption and solvation energies (ΔE_{ad} and ΔE_{sol}) computed via geometry optimizations at all adsorption sites probed during the AIMD simulations. Additional to the VASPsol results (see main text) the optimized energies in Quantum ESPRESSO / Environ (QE-SCCS) are depicted. The overall site-occupation ratio r_{site} and the residence time τ during the AIMD simulations for each site are shown as well. See Fig. S3 for an explanation of the site labels.

	$\Delta E_{\mathrm{ad}}^{\mathrm{VASPsol}}$	$\Delta E_{\mathrm{sol}}^{\mathrm{VASPsol}}$	$\Delta E_{\mathrm{ad}}^{\mathrm{QE\text{-}SCCS}}$	$\Delta E_{\mathrm{sol}}^{\mathrm{QE\text{-}SCCS}}$	r_{site}	τ (ps)
	OH / Cu(111)					
bridge	0.03	-0.08	-0.03	-0.09	0.58	501.53
hollow3-a	0.07	-0.08	-0.07	-0.08	0.13	422.92
hollow3-b	0.07	-0.08	-0.06	-0.08	0.12	342.83
top	0.17	-0.09	0.38	-0.16	0.17	457.88
	CO / Cu(111)					
hollow3-b	-0.88	-0.02	-0.78	-0.00	0.22	434.52
hollow3-a	-0.87	-0.02	-0.78	-0.00	0.28	423.74
top	-0.85	-0.01	-0.81	0.01	0.04	411.40
bridge	-0.85	-0.01	-0.81	0.01	0.46	301.15
	OH / Au(111)					
bridge	1.00	-0.07	0.98	-0.08	0.30	344.27
hollow3-b	1.00	-0.07	0.97	-0.08	0.03	299.28
hollow3-a	1.04	-0.07	1.08	-0.02	0.14	433.95
top	1.14	-0.18	1.15	-0.15	0.54	787.82
	CO / Au(111)					
top	-0.39	-0.00	-0.39	-0.00	0.33	747.31
hollow3-b	-0.37	0.01	-0.37	0.01	0.13	340.05
bridge	-0.37	0.01	-0.36	0.01	0.47	428.55
hollow3-a	-0.20	-0.03	-0.36	0.01	0.07	290.42
	OH / Pt(111)					
top	0.62	-0.12	0.62	-0.14	0.99	1801.37
bridge	0.71	-0.13	0.65	-0.13	0.01	0.00
	CO / Pt(111)					
bridge	-1.89	-0.00	-1.85	-0.03	0.64	441.08
hollow3-a	-1.89	-0.00	-1.84	-0.03	0.25	513.82
hollow3-b	-1.88	-0.01	-1.84	-0.03	0.11	837.68

IV Detailed tables for competitive water adsorption

Table S5: H_2O adsorption statistics for Cu(211) with and without (clean) the presence of adsorbates including the site-resolution. Displayed are the average number of H_2O molecules adsorbed ($\langle n_{\mathrm{ad}}^{\mathrm{H_2O}} \rangle$), the frequency of H_2O adsorption ($f_{\mathrm{ad}}^{\mathrm{H_2O}}$) and the average residence time of H_2O molecules ($\langle \tau \rangle$) on the surface. Sites with less than 1 % H_2O adsorbed are not shown. See Fig. S3 for an explanation of the site labels.

site	$\langle n_{\mathrm{ad}}^{\mathrm{H_2O}} \rangle$	f_{ad} (ps^{-1})	$\langle \tau \rangle$ (fs)
clean Cu(211)			
total	1.68	2.95	599.2
top-c	1.53	1.25	1262.2
bridge-e	0.08	0.70	124.4
bridge-f	0.05	0.59	128.2
bridge-d	0.01	0.18	48.1
hollow4	0.01	0.10	81.5
OH / Cu(211)			
total	1.23	2.15	589.2
top-c	0.89	0.17	5182.4
top-b	0.27	0.70	418.4
bridge-e	0.03	0.50	72.1
bridge-f	0.01	0.12	106.1
bridge-b	0.01	0.29	37.5
bridge-d	0.01	0.16	65.0
CO / Cu(211)			
total	1.23	2.35	540.4
top-c	1.08	0.69	1601.7
bridge-e	0.08	0.73	121.0
top-b	0.03	0.13	223.7
bridge-f	0.02	0.43	61.1
bridge-d	0.01	0.23	60.3

Table S6: H_2O adsorption statistics for Cu(211) with and without (clean) the presence of adsorbates including the site-resolution. Displayed are the average number of H_2O molecules adsorbed ($\langle n_{\mathrm{ad}}^{\mathrm{H_2O}} \rangle$), the frequency of H_2O adsorption ($f_{\mathrm{ad}}^{\mathrm{H_2O}}$) and the average residence time of H_2O molecules ($\langle \tau \rangle$) on the surface. Sites with less than 1 % H_2O adsorbed are not shown. See Fig. S3 for an explanation of the site labels.

site	$\langle n_{\mathrm{ad}}^{\mathrm{H_2O}} \rangle$	f_{ad} (ps^{-1})	$\langle \tau \rangle$ (fs)
CHO / Cu(211)			
total	1.22	2.18	595.6
top-c	0.91	0.77	1260.4
bridge-e	0.20	0.60	355.1
top-b	0.08	0.32	261.5
bridge-f	0.01	0.16	97.5
bridge-b	0.01	0.14	37.1
COH / Cu(211)			
total	0.34	0.51	697.1
top-c	0.30	0.19	1602.6
bridge-e	0.01	0.12	130.9
top-b	0.01	0.06	239.9
bridge-f	0.01	0.07	145.6
OCCHO / Cu(211)			
total	2.15	3.11	717.8
top-b	1.04	0.58	1900.8
top-c	0.93	0.23	4096.0
bridge-e	0.08	0.40	203.2
bridge-b	0.04	0.89	58.2
bridge-c	0.02	0.39	65.8
bridge-f	0.01	0.15	132.7
bridge-d	0.01	0.20	68.2

Table S7: H_2O adsorption statistics for Cu(111) with and without (clean) the presence of adsorbates including the site-resolution. Displayed are the average number of H_2O molecules adsorbed ($\langle n_{\mathrm{ad}}^{\mathrm{H_2O}} \rangle$), the frequency of H_2O adsorption ($f_{\mathrm{ad}}^{\mathrm{H_2O}}$) and the average residence time of H_2O molecules ($\langle \tau \rangle$) on the surface. Sites with less than 1 % H_2O adsorbed are not shown. See Fig. S3 for an explanation of the site labels.

site	$\langle n_{\mathrm{ad}}^{\mathrm{H_2O}} \rangle$	f_{ad} (ps^{-1})	$\langle \tau \rangle$ (fs)
clean Cu(111)			
total	1.42	6.35	240.1
top	1.13	2.08	577.6
bridge	0.23	3.21	79.7
hollow3-b	0.04	0.65	59.7
hollow3-a	0.02	0.41	67.4
OH / Cu(111)			
total	1.11	3.99	300.9
top	0.97	1.87	563.7
bridge	0.11	1.70	72.5
hollow3-b	0.01	0.21	62.2
hollow3-a	0.01	0.21	53.5
CO / Cu(111)			
total	1.18	4.82	264.1
top	0.99	1.78	598.4
bridge	0.16	2.40	70.5
hollow3-b	0.02	0.38	61.9
hollow3-a	0.01	0.26	52.0

Table S8: H_2O adsorption statistics for Au(111) with and without (clean) the presence of adsorbates including the site-resolution. Displayed are the average number of H_2O molecules adsorbed ($\langle n_{\mathrm{ad}}^{\mathrm{H_2O}} \rangle$), the frequency of H_2O adsorption ($f_{\mathrm{ad}}^{\mathrm{H_2O}}$) and the average residence time of H_2O molecules ($\langle \tau \rangle$) on the surface. Sites with less than 1 % H_2O adsorbed are not shown. See Fig. S3 for an explanation of the site labels.

site	$\langle n_{\mathrm{ad}}^{\mathrm{H_2O}} \rangle$	f_{ad} (ps^{-1})	$\langle \tau \rangle$ (fs)
clean Au(111)			
total	0.07	1.30	57.9
top	0.05	0.93	61.1
bridge	0.01	0.22	48.0
hollow3-b	0.01	0.11	64.0
OH / Au(111)			
total	1.04	9.98	122.5
top	0.60	4.73	150.0
bridge	0.30	3.62	96.6
hollow3-a	0.09	1.12	101.6
hollow3-b	0.04	0.51	97.2
CO / Au(111)			
total	0.03	0.56	48.2
top	0.02	0.38	53.0
bridge	0.01	0.13	43.9

Table S9: H_2O adsorption statistics for Pt(111) with and without (clean) the presence of adsorbates including the site-resolution. Displayed are the average number of H_2O molecules adsorbed ($\langle n_{\mathrm{ad}}^{\mathrm{H_2O}} \rangle$), the frequency of H_2O adsorption ($f_{\mathrm{ad}}^{\mathrm{H_2O}}$) and the average residence time of H_2O molecules ($\langle \tau \rangle$) on the surface. Sites with less than 1 % H_2O adsorbed are not shown. See Fig. S3 for an explanation of the site labels.

site	$\langle n_{\mathrm{ad}}^{\mathrm{H_2O}} \rangle$	f_{ad} (ps^{-1})	$\langle \tau \rangle$ (fs)
clean Pt(111)			
total	1.83	1.44	1327.7
top	1.81	0.98	1931.0
bridge	0.02	0.40	53.1
OH / Pt(111)			
total	1.05	1.19	945.5
top	1.04	1.01	1100.9
bridge	0.01	0.16	54.2
CO / Pt(111)			
total	1.92	2.48	806.6
top	1.87	1.23	1577.4
bridge	0.04	1.07	43.5

V Solvation energy relationships

Va Correlations to deviation of continuum solvation energies

The correlation against hydrogen bonding n_{Hbond} and competitive water adsorption $\Delta\langle n_{\mathrm{ad}}^{\mathrm{H_2O}}\rangle$ of the solvation energy (see main text), equally fits to the difference of solvation energies $\Delta\Delta E_{\mathrm{solv}}^{\text{aimd-impl}}$ between AIMD and continuum solvation. As depicted in Fig. S4, the $\Delta\Delta E_{\mathrm{solv}}^{\text{aimd-impl}}$ gives a clear cut correlation with both quantities. The corresponding linear relationships follow for hydrogen bonding as $f = 1.57\,\mathrm{eV} - (0.74 \cdot \langle n_{\mathrm{Hbond}}\rangle)\,\mathrm{eV}$ and for competitive water adsorption as $f = -0.15\,\mathrm{eV} - (0.79 \cdot \Delta\langle n_{\mathrm{ad}}^{\mathrm{H_2O}}\rangle)\,\mathrm{eV}$.

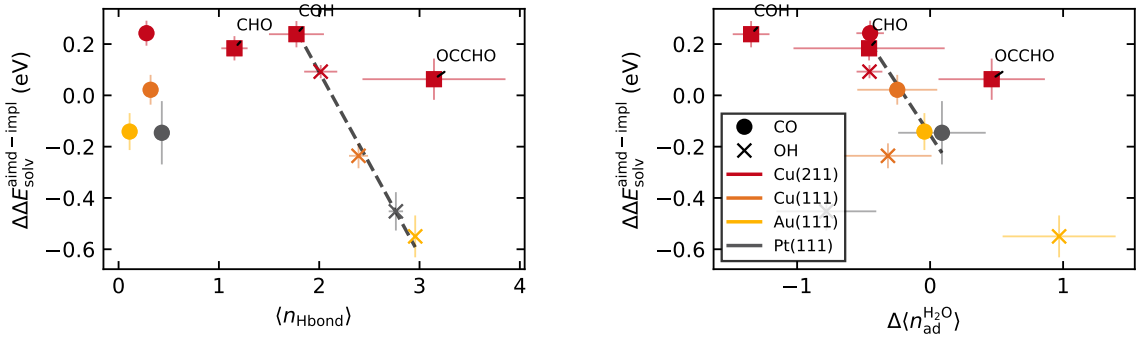

Figure S4: Difference of the solvation energy between AIMD and continuum solvation $\Delta\Delta E_{\mathrm{solv}}^{\text{aimd-impl}}$ against the average number of Hbonds $\langle n_{\mathrm{Hbond}}\rangle$ (left) and against the difference in average number of adsorbed water molecules in presence of an adsorbate against the clean surface $\Delta\langle n_{\mathrm{ad}}^{\mathrm{H_2O}}\rangle$ (right). Apparent correlations (see text) are indicated by the dark dashed lines.

Vb Towards the prediction of hydrogen bonding and water adsorption at the mtal/water interface

The quantified linear correlation of solvation energies with the hydrogen bonding $\langle n_{\mathrm{Hbond}}\rangle$ and competitive water adsorption $\Delta\langle n_{\mathrm{ad}}^{\mathrm{H_2O}}\rangle$ suggest a underlying physical relationship. This relationship may in turn be exploited to predict accurate solvation energies without the need for costly AIMD simulations. In order to do so, $\langle n_{\mathrm{Hbond}}\rangle$ and $\langle n_{\mathrm{ad}}^{\mathrm{H_2O}}\rangle$ need to be predictable from reliably determinable descriptors. We correlate $\langle n_{\mathrm{Hbond}}\rangle$ and $\Delta\langle n_{\mathrm{ad}}^{\mathrm{H_2O}}\rangle$ (or

$\langle n_{\mathrm{ad}}^{\mathrm{H_2O}} \rangle$) against a number of descriptors including surface dipole moments, Bader charges, workfunction and solvation/adsorption energies from microsolvation models. For clarity we only present the descriptors showing highest correlations.

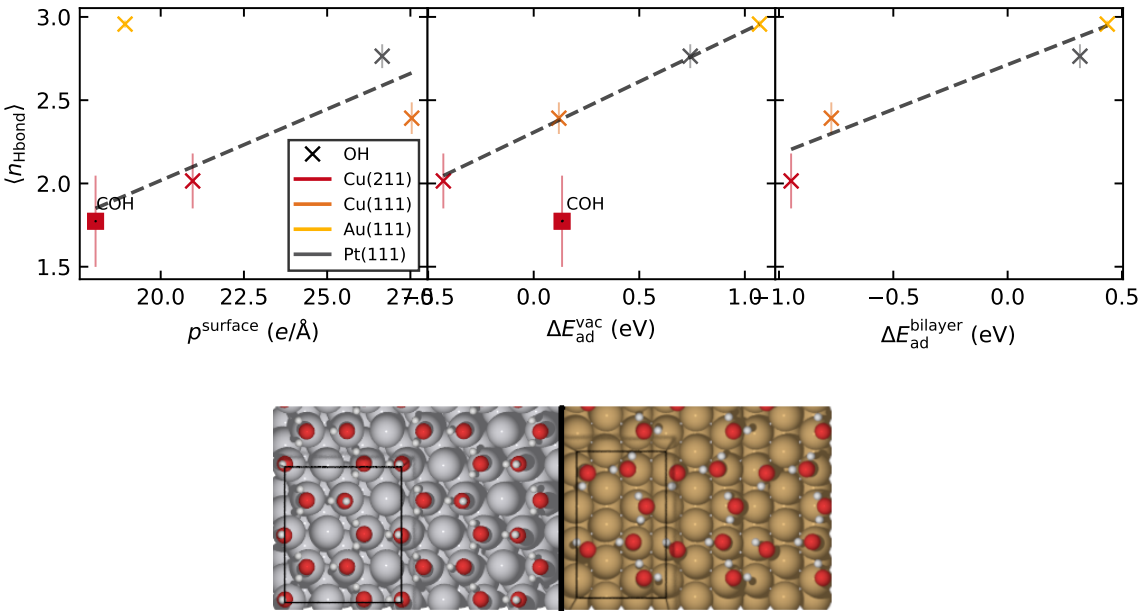

Figure S5: (top) Correlation of hydrogen bonding with the surface dipole moment p^{surface} (left), adsorption energy at the metal/vacuum interface $\Delta E_{\mathrm{ad}}^{\mathrm{vac}}$ (center) and adsorption energy in presence of a complete ice-like bilayer $\Delta E_{\mathrm{ad}}^{\mathrm{bilayer}}$ (right). The relations are depicted for *OH and *COH. Apparent correlations (see text) are indicated by the dark dashed lines. (bottom) Examples of the water bilayer structure incorporating *OH on Pt(111) (left) and Cu(211) (right).

For the hydrogen bonding we find some correlation with the surface dipole moment of the adsorbate at the metal/vacuum interface and adsorption energies determined in vacuum and in presence of a static water bilayer. As shown in Fig. S5, the surface dipole moment correlates $\langle n_{\mathrm{Hbond}} \rangle$ across the adsorbates *OH and *COH and metal facets Cu(211), Cu(111), Pt(111) with a moderate error of $\approx 0.1\,\mathrm{eV}$. The sole but significant outlier with a deviation according to $\approx 0.8\,\mathrm{eV}$ is *OH on Au(111). The physical explanation for Au(111) being an outlier is likely due to the fundamental change in the metal/water interface. Originating in the "anchoring effect" of the *OH group, which is not as dramatic for the other surfaces, the water is significantly closer to the Au(111) surface changing the apparent surface dipole

in the AIMD simulation (see Sec. III A in the main text). This deviation disqualifies the surface dipole moment as a reliable descriptor. The adsorption energies among the *OH adsorbates at the metal/vacuum interface scale with $\langle n_{\mathrm{Hbond}} \rangle$. This trend does, however, exclude *COH on Cu(211) and may thus only be relevant among same types of adsorbates – similar to the general scaling relations for adsorption energies.[8] We can formulate a model to predict solvation energies specifically for *OH on metal surfaces from this correlation in combination with our solvation energy-$\langle n_{\mathrm{Hbond}} \rangle$ relationship (see main text). A function for the solvation energy of *OH ($\Delta E_{\mathrm{solv}}^{^*\mathrm{OH}}$) follows as $\Delta E_{\mathrm{solv}}^{^*\mathrm{OH}} = -0.22\,eV - 0.44 \cdot \Delta E_{\mathrm{ad}}^{\mathrm{vac},^*\mathrm{OH}}$. This function yields an increasing solvation energy with a weaker binding strength of the *OH to the metal surface. Finally, a correlation of $\langle n_{\mathrm{Hbond}} \rangle$ to adsorption energies in the presence of a static bilayer also retain the previous trend. However, the setup of a static bilayer is in no way straight forward. While a hexagonal bilayer is commonly used on a Pt(111) surface[9] its realization is not straight forward on other metals or facets as shown for the example of Cu(211) in Fig. S5. A sampling problem follows this issue. As a consequence, the data suffers from considerable scatter and an unsystematic "correction" follows for the adsorption energies. The latter, leads to a slight improvement for Pt(111) and Au(111) but a clear worsening for Cu(111) and Cu(211) in comparison to the AIMD values (see main text). Further, we could not stabilize *COH in presence of a static water bilayer. Such practical issues disqualify static water layer models for the reliable prediction of specific properties of metal/water interfaces.

In the case of the average water adsorption $\langle n_{\mathrm{ad}}^{\mathrm{H_2O}} \rangle$ at the pure metal/water interface, we find very good correlation of its top-site normalized value with the (most stable) adsorption energy of a single water molecule at the metal/vacuum interface as shown in Fig. S6. While this result is quite intuitive, it confirms hydrophilicity as an atomistic/microscopic property. Consolidating the competitive water adsorption $\Delta\langle n_{\mathrm{ad}}^{\mathrm{H_2O}} \rangle$ is, however, at this point unclear. We only can show a weak correlation between the difference in binding energy of an adsorbate and a water molecule (c.f. Fig. S6). Excluded from this correlation is CO on Au(111).

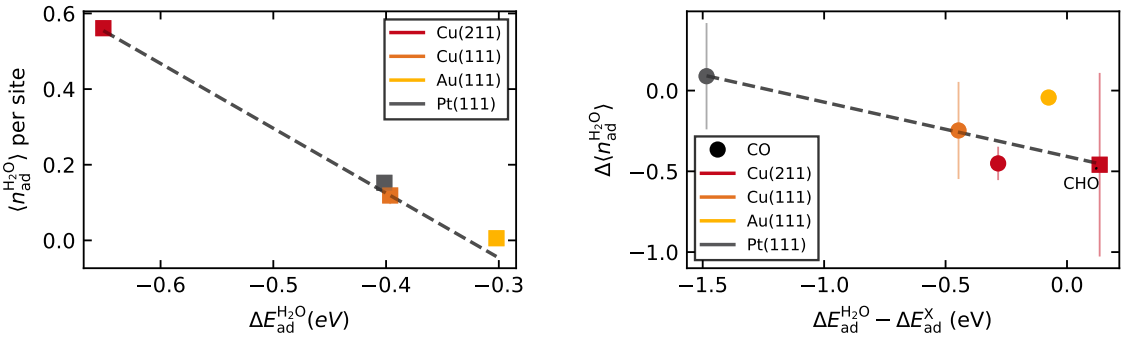

Figure S6: (left) Correlation for the amount of the top-site normalized water adsorption $\langle n_{\mathrm{ad}}^{\mathrm{H_2O}}\rangle$ with the lowest adsorption energy of a single water molecule at the metal/vacuum interface ($\Delta E_{\mathrm{ad}}^{\mathrm{H_2O}}$). (right) Correlation of the difference of water adsorption upon presence of an adsorbate ($\Delta\langle n_{\mathrm{ad}}^{\mathrm{H_2O}}\rangle$) against the difference in adsorption energy of a single water molecule and the respective adsorbate x ($\Delta E_{\mathrm{ad}}^{\mathrm{H_2O}} - \Delta E_{\mathrm{ad}}^{\mathrm{x}}$).

It should be noted, that the latter outlier does not show any water adsorption ($\langle n_{\mathrm{ad}}^{\mathrm{H_2O}}\rangle$=0). In such a case, competitive water adsorption does not play a role. To capture this exception a $\langle n_{\mathrm{ad}}^{\mathrm{H_2O}}\rangle$=0 criterion would be needed as an additional descriptor for the prediction of competitive water adsorption.

References

(1) Gunceler, D.; Letchworth-Weaver, K.; Sundararaman, R.; Schwarz, K. A.; Arias, T. The importance of nonlinear fluid response in joint density-functional theory studies of battery systems. *Modelling Simul. Mater. Sci. Eng.* **2013**, *21*, 074005.

(2) Mathew, K.; Hennig, R. G. Implicit self-consistent description of electrolyte in plane-wave density-functional theory. *arXiv preprint* **2016**,

(3) Giannozzi, P. et al. QUANTUM ESPRESSO: a modular and open-source software project for quantum simulations of materials. *J. Phys. Condens. Matter* **2009**, *21*, 395502.

(4) Andreussi, O.; Dabo, I.; Marzari, N. Revised self-consistent continuum solvation in electronic-structure calculations. *J. Chem. Phys.* **2012**, *136*.

(5) Hammer, B.; Hansen, L. B.; Nørskov, J. K. Improved adsorption energetics within density-functional theory using revised Perdew-Burke-Ernzerhof functionals. *Phys. Rev. B* **1999**, *59*, 7413.

(6) Grimme, S.; Antony, J.; Ehrlich, S.; Krieg, H. A consistent and accurate ab initio parametrization of density functional dispersion correction (DFT-D) for the 94 elements H-Pu. *J. Chem. Phys.* **2010**, *132*, 154104.

(7) Grimme, S. Density functional theory with London dispersion corrections. *Wiley Interdiscip. Rev.: Comput. Mol. Sci.* **2011**, *1*, 211–228.

(8) Abild-Pedersen, F.; Greeley, J.; Studt, F.; Rossmeisl, J.; Munter, T.; Moses, P. G.; Skulason, E.; Bligaard, T.; Nørskov, J. K. Scaling properties of adsorption energies for hydrogen-containing molecules on transition-metal surfaces. *Phys. Rev. Lett.* **2007**, *99*, 016105.

(9) Tripković, V.; Skúlason, E.; Siahrostami, S.; Nørskov, J. K.; Rossmeisl, J. The oxygen reduction reaction mechanism on Pt(111) from density functional theory calculations. *Electrochimica Acta* **2010**, *55*, 7975 – 7981.